HHS Public Access

Author manuscript

Biochemistry. Author manuscript; available in PMC 2016 May 12.

Published in final edited form as:

Biochemistry. 2015 May 12; 54(18): 2874–2884. doi:10.1021/acs.biochem.5b00171.

SPECTROSCOPIC AND COMPUTATIONAL INVESTIGATION OF THE H155A VARIANT OF CYSTEINE DIOXYGENASE: GEOMETRIC AND ELECTRONIC CONSEQUENCES OF A THIRD-SPHERE AMINO ACID SUBSTITUTION

Elizabeth J. Blaesi[1,+], **Brian G. Fox**[2], and **Thomas C. Brunold**[1,*]

[1]Department of Chemistry, University of Wisconsin-Madison, Madison, WI 53706

[2]Department of Biochemistry, University of Wisconsin-Madison, Madison, WI 53706

Abstract

Cysteine dioxygenase (CDO) is a mononuclear, non-heme iron(II)-dependent enzyme that utilizes molecular oxygen to catalyze the oxidation of L-cysteine (Cys) to cysteine sulfinic acid. X-ray crystal structures of CDO have revealed that unusual structural motifs are present in both the first and the second coordination spheres of the Fe center, including a three-histidine metal binding site and a cysteine-tyrosine crosslink that is formed post-translationally. Although the kinetic consequences of various outer-sphere amino acid substitutions have previously been assessed, the effects of these substitutions on the geometric and electronic structures of the active site remained largely unexplored. In this work, we have performed a spectroscopic and computational characterization of the H155A CDO variant, which was previously shown to display a ~100-fold decreased rate of Cys oxidation relative to wild-type (WT) CDO. Magnetic circular dichroism and electron paramagnetic resonance spectroscopic data indicate that the His155→Ala substitution has a significant effect on the electronic structure of the Cys-bound Fe(II)CDO active site. An analysis of these data within the framework of quantum mechanics/molecular mechanics (QM/MM) and single-point density functional theory calculations reveals that Cys-bound H155A Fe(II)CDO possesses a six-coordinate Fe(II) center, differing from the analogous WT CDO species by the presence of an additional water ligand. The enhanced affinity of the Cys-bound Fe(II) center for a sixth ligand in the H155A CDO variant likely stems from the increased conformational freedom of the cysteine-tyrosine crosslink in the absence of the H155 imidazole ring. Despite these differences between the WT and H155A Cys-Fe(II)CDO species, the nitrosyl adducts of Cys- and Sec-bound Fe(II)CDO [which mimic the (O_2/Cys)-CDO intermediate] are essentially unaffected by the H155A substitution, suggesting that the primary role played by the H155 side chain in CDO catalysis is to discourage the binding of a water molecule to the Cys-bound Fe(II)CDO active site.

Cysteine dioxygenase (CDO) is a mononuclear, non-heme iron enzyme that catalyzes the oxidation of exogenous cysteine (Cys) by O_2 to cysteine sulfinic acid with nearly complete substrate fidelity.[1–3] This conversion represents the only oxidative degradation pathway for

*Corresponding Author 1101 University Ave, Madison, WI 53706, Phone: (608) 265-9056, Fax: (608) 262-6143, brunold@chem.wisc.edu.

+Present address: 317 Chemistry Building, Pennsylvania State University, University Park, PA 16802

Cys,[4] and it has been proposed that CDO is ultimately responsible for the majority of taurine produced in mammals.[5] Malfunctioning CDO has been implicated in a variety of neurological disorders, such as Alzheimer's, Parkinson's and motor neuron diseases.[6–10] Additionally, recent studies have shown that the *CDO1* gene is down-regulated through the methylation of its promoter in certain forms of human cancers (including breast and colorectal), and that tumor growth may be suppressed through the restoration of the normal levels of *CDO1* expression.[11, 12]

The first CDO crystal structure (published in 2006[13]) revealed several unique geometric features of this enzyme, including an intramolecular cross-link between residues C93 and Y157, as well as a rare 3-histidine (3His) facial ligation sphere about the iron center in the resting state of the enzyme. Subsequent crystal structures have provided evidence for bidentate binding of the substrate Cys through its thiolate and amino groups,[14] and a direct Fe–S bonding interaction [or Fe–Se interaction in the case of CDO incubated with the substrate analogue selenocysteine (Sec)] was confirmed through resonance Raman and magnetic circular dichroism (MCD) spectroscopic studies.[15] Recent work by our group has suggested that although Cys-bound Fe(II)CDO features a five-coordinate active site (as revealed by multiple X-ray crystal structures[13, 14, 16]), the Fe center of Cys-bound Fe(III)CDO additionally possesses a hydroxide ligand to adopt a six-coordinate, distorted octahedral coordination envorinment.[17]

In an effort to obtain molecular-level insight into the CDO reaction mechanism, analogues for dioxygen (including NO, CN^-, and superoxide) have been used with great success to mimic viable O_2-bound intermediates. Electron paramagnetic resonance (EPR) spectroscopy has been employed in three such studies, one of which focused on the transient superoxide adduct of Cys-bound Fe(III)CDO.[18] This (superoxo/Cys)-Fe(III)CDO adduct was found to exhibit an EPR spectrum that could successfully be simulated using parameters for either an S=3 or an S=2 spin system. In a separate study, the EPR spectrum of the (CN^-/Cys)-Fe(III)CDO adduct was found to change slightly in response to C93-Y157 cross-link formation, with the fully cross-linked protein exhibiting a larger *g*-spread than the non-cross-linked enzyme.[3] The first application of EPR spectroscopy to CDO revealed that the nitrosyl adduct of Cys-bound Fe(II)CDO represents a rare S=1/2 $\{FeNO\}^7$ species, as opposed to an S=3/2 species as is typically observed for non-heme iron enzymes.[19] To further characterize this unusual $\{FeNO\}^7$ species, a combined spectroscopic and computational approach was utilized, which revealed that the presence of a strongly π-donating thiolate ligand in conjunction with the neutral 3His facial ligation to the Fe center are key contributors to the stabilization of the S=1/2 state [where a low-spin Fe(II) ion is ligated by an $NO^\bullet$] over the S=3/2 state [featuring a high-spin Fe(III) ion coupled antiferromagnetically to NO^-]. The spectroscopically validated computational methodology developed in this work was then used to propose a mechanism for O_2 activation by CDO in which the iron oxidation state never exceeds +3 and the substrate Cys acts as a redox non-innocent ligand.[20] In support of this proposal, a subsequent experimental and computational study revealed that the same computational methodology could be used successfully to describe the geometric and electronic properties of the different species formed upon incubation of CDO with azide.[21]

Although the effects of substituting various outer-sphere residues on the catalytic properties of CDO have been assessed in several studies,[3, 16, 22] in all but one case these variants have not yet been characterized spectroscopically to probe their perturbed geometric and electronic active site structures.[3] To overcome these deficiencies, we have initiated combined spectroscopic and computational studies of CDO variants for identifying specific roles performed by individual outer-sphere residues in the catalytic cycle. In the present study, the H155 residue was replaced by an alanine in order to examine how the imidazole side-chain influences the properties of the CDO active site and its interaction with the Cys and O_2 substrates.

Residue H155 is a member of the S153-H155-Y157 (mouse CDO numbering) catalytic triad motif that is highly conserved among CDO enzymes. The presence of this motif has been successfully used to screen protein sequences in order to identify members of the cupin superfamily with CDO activity, including several previously unknown bacterial homologs.[23] X-ray crystallographic data of Cys-bound CDO revealed these three residues engage in an extended hydrogen bonding network, with the oxygen atom of the S153 side chain residing within 2.65 Å of the Nε atom of H155 and the Nδ atom of H155 located 2.77 Å from the Y157 oxygen atom (see Figure 1).[14] As the Y157 phenol is in turn located within hydrogen-bonding distance of the carboxylic acid group of the substrate Cys, the interactions between H155 and neighboring residues may exert significant control over the positioning of the Cys substrate at the active site. Additionally, H155 is one of the few acidic active site residues available to act as a proton donor and may thus be involved in the putative proton transfer to an intermediate that occurs between O_2 activation and product release.[24] Consistent with these predictions, it was found that the specific activity of the H155A CDO variant is significantly lower than that of the wild-type (WT) enzyme ($k_{cat} < 0.1$ vs. 8.6 s^{-1}, respectively).[3] Moreover, a K_M for Cys binding to the variant enzyme could not be determined as no saturation was observed even at 25 mM Cys.[3]

2. Experimental Procedures

2.1 Gene Expression and Protein Purification

The wild-type (WT) CDO gene from *Mus musculus* was cloned into a pVP16 vector with maltose binding protein (MBP) as an N-terminal fusion protein tag, as previously described.[13] To generate the H155A mutant plasmid DNA, polymerase chain reaction (PCR) was performed with a Herculase II kit on the WT CDO-containing vector, using forward and reverse mutagenic primers (25 nucleotides in length, with the mutated codon centered in the primer sequences) where the nucleotides describing the H155 codon were substituted appropriately to create the H155A mutant plasmid DNA. The resultant DNA was treated with the DpnI restriction enzyme for one hour at 37 °C to destroy the original WT CDO DNA template. Competent JM109 cells were exposed to the mutant plasmid, heat shocked, and plated onto a lysogeny broth/agar medium containing ampicillin (to which the pVP16 plasmid confers resistance). Individual bacterial colonies resultant from this process were separately grown further in 10 mL cultures overnight at 37 °C. The plasmid DNA from the cells in each culture was isolated by use of a QIAprep kit, and sequenced using a Big Dye kit in conjunction with the Sanger sequencing method (at the University of Wisconsin-

Madison Biotechnology Center) to ensure the mutagenesis was both successful and selective for the desired mutation. Plasmids with alternative, extra, or no mutations were discarded.

Expression from the H155A plasmid and purification of the corresponding H155A protein variant were conducted in the same manner as for the WT version of this protein, which has been described elsewhere.[20] In brief, CDO was expressed in *Escherichia coli* BL21(DE3) cells through induction with isopropyl β-D-1-thiogalactopyranoside (IPTG). The protein purification was conducted through the use of pulsed sonication cell disruption and three separatory columns, namely diethylaminoethyl cellulose (DEAE) anion exchange, amylose affinity (to bind the fusion protein exclusively), and size-exclusion (Sephacryl S-100) columns. After elution from the amylose column, but before application to the S-100 column, fractions containing the MBP-CDO fusion protein were incubated overnight with tobacco etch virus to release the MBP affinity tag from the target CDO protein.

Similar to the WT enzyme,[19] H155A CDO was isolated with iron occupying only a fraction of active sites (~20%) and with an Fe(II):Fe(III) ratio of ~45:55. The activity of the as-isolated H155A CDO variant was verified by use of a qualitative thin-layer chromatography-based assay, as described elsewhere (data not shown).[15] It has been shown previously that the fraction of CDO protein molecules containing of the C93-Y157 thioether cross-link can be estimated on the basis of the double-band pattern observed on an SDS-PAGE gel.[25] Although a gel previously published by Pierce and coworkers did not exhibit the lower band associated with cross-linked H155A CDO,[3] in our hands a portion of the as-isolated variant clearly contains this C-Y cross-link, albeit in somewhat lower yield than the WT protein (see Figure S1, Supporting Information). However, because cross-linked CDO is more stable than protein lacking the crosslink[22] and cross-link formation requires the presence of iron at the active site,[26] it is reasonable to assume that the majority of iron-bound active sites in our H155A CDO samples were in the cross-linked form.

2.2 Sample Preparation

The iron(II) and iron(III) content of the protein was determined through a colorimetric assay using the iron chelator tripyridyl triazine (TPTZ) and ε_{590}=22.1 mM^{-1} cm^{-1}.[27] The assay was performed both in the presence and the absence of a reductant (hydroxylamine) to determine the proportion of Fe(II) vs. Fe(III) initially present. As neither the variant nor WT CDO protein had iron bound at all active sites, the concentration of protein cited herein refers to the Fe-bound fraction, and not that of the total protein. Samples used for spectroscopy were prepared anaerobically via either Schlenk line or glove box methods, and contained a five-fold excess of L-cysteine (Cys) or L-selenocysteine (Sec) over Fe-bound CDO. Sec was prepared through the anaerobic reduction of selenocystine with tris(2-carboxyethyl)phosphine (TCEP). The nitrosyl adducts of Cys- or Sec-bound Fe(II)CDO were prepared through the introduction of NO gas (generated through the anaerobic reaction of aqueous cupric chloride, sodium nitrite, and ascorbic acid) to the sample vial headspace, as described previously.[20] Where applicable, sodium azide was added in a 200-fold molar excess over Fe-bound CDO. Samples for low-temperature (LT) Abs and MCD studies also contained 55% (v/v) glycerol as a glassing agent.

2.3 Spectroscopy

Room temperature absorption (RT Abs) spectra were obtained using a Varian Cary 5e spectrophotometer while the sample compartment was purged with N_2(g). LT Abs and MCD spectra were collected with a Jasco J-715 spectropolarimeter in conjunction with an Oxford Instruments SM4000-8T magnetocryostat. The MCD spectra presented herein were obtained by taking the difference between the spectra obtained with the magnetic field aligned parallel and antiparallel to the light propagation axis to eliminate contributions from the CD background and glass strain.

X-Band EPR spectra were collected using a Bruker ESP 300E spectrometer equipped with a Varian EIP model 625A continuous wave frequency counter. The sample temperature was maintained at 20 K by an Oxford ESR 900 continuous flow liquid He cryostat that was regulated by an Oxford ITC temperature controller. Spectra were simulated using the EasySpin program by Stoll and Schweiger.[28]

2.4 Computations

Initial coordinates for the whole protein quantum mechanics/molecular mechanics (QM/MM) geometry optimizations were generated as previously described.[20] Guided by a previous characterization of Cys-bound WT Fe(III)CDO, our models of both the Cys and Sec adducts of Fe(III)CDO additionally featured a hydroxide anion bound to the Fe center.[21] In preparing (H_2O/Cys) and (H_2O/Sec)-Fe(II)CDO models, a water molecule from elsewhere in the QM region was moved to within bonding distance of the Fe center, so as to maintain the same total number of atoms in the QM region for the five- and six-coordinate models. To generate initial models for the H155A CDO variant, the crystal structure coordinates were manually altered by replacing the side chain of residue 155 with an alanine side chain prior to any geometry optimization step. For all optimizations, the QM/MM package as implemented in Gaussian09[29] was utilized in conjunction with Amber force field[30] parameters for MM region atoms and density functional theory (DFT) in combination with the B3LYP[31, 32] functional for QM region atoms. The 6-31G[33] basis set was used for all QM atoms, with the exception of iron, all atoms immediately coordinated to it, and any exogenous water, hydroxide, nitric oxide, or dioxygen ligand, for which TZVP[34] was used instead. After a converged whole-protein structure was obtained, residues H86, H88, and H140, as well as iron and any exogenous ligands were excised and the endogenous amino acid residues were capped with methyl groups at the beta carbon with C–H bond distances of 1.1 Å. These active site models were then used for further calculations as described below (atomic coordinates for all of these models are provided in Tables S4-S14 of the Supporting Information).

Spin-unrestricted DFT calculations were performed in Orca 2.9.1[35] using the same functional and basis sets as were used for the QM portion of the QM/MM optimization. PyMOL version 1.5.0.4[36] was utilized to generate isosurface plots of the calculated molecular orbitals (MOs) using an isodensity value of 0.05 au. Because previous attempts to utilize time-dependent DFT for predicting the absorption spectra of CDO species proved unsuccessful,[21] electronic transition energies and Abs intensities were computed by employing the semi-empirical INDO/S-CI method as implemented in Orca 3.0.2. Spin-

unrestricted Hartree-Fock self-consistent-field calculations were converged on the S=2 [Fe(II)CDO species] and S=5/2 [Fe(III)CDO species] ground states, which then served as the reference states for configuration interaction calculations. In each case, electronic transition energies and intensities were computed for the 60 lowest-energy excited states, and Abs spectra were simulated by assuming that each electronic transition gives rise to a Gaussian band with a constant bandwidth.

In the DFT-based calculation of EPR parameters, the coupled-perturbed self-consistent field (SCF) approach was utilized as implemented in Orca 2.9.1, using the B3LYP hybrid functional and the CP(PPP)[37, 38] basis set for iron, IGLO-III[39] for the nitrogen of the NO, and TZVP[34] for the remaining atoms. All orbitals within ±100 Hartrees of the HOMO-LUMO gap were considered, and the origin of the g-tensor was set at the center of the electronic charge. A high-resolution radial grid with an integration accuracy of 7.0 was used for the Fe atom and the nitrogen of the NO ligand (if present). Both spin-spin and spin-orbit contributions to the D-tensor were considered for S > 1/2 systems.

3. Spectroscopic Results

3.1 Cys and Sec adducts of H155A CDO

The Abs and MCD spectra of as-isolated WT CDO in the presence of Cys and Sec were previously published and analyzed within the framework of resonance Raman experiments and computational work.[15] Although the as-isolated protein contains a mixture of Fe(II)- and Fe(III)CDO, the Abs and MCD features exhibited by the corresponding Cys adducts occur in distinct spectral regions and can thus be probed simultaneously. Specifically, in the case of the Cys-bound CDO species, the Abs features at 32,000 and 15,700 cm^{-1} (along with their respective MCD features) have been shown to arise from S_{Cys}→Fe(II) and S_{Cys}→Fe(III) charge transfer (CT) transitions, respectively. Similarly, the Abs and MCD features at 30,000 and 13,250 cm^{-1} displayed by the Sec-bound CDO species were assigned as Se_{Sec}→Fe(II) and Se_{Sec}→Fe(III) CT transitions, respectively. The red-shift of the Sec-based CT features relative to their Cys-derived counterparts was attributed to a destabilization of the occupied Se_{Sec}-based frontier molecular orbitals with respect to their S_{Cys} counterparts.[15]

As is the case for WT CDO, as-isolated H155A CDO contains a mixture of Fe(II)- and Fe(III)-bound active sites in a ratio of ~45:55. Upon exposure of the variant to Cys, features similar to those observed in the MCD spectrum of as-isolated WT CDO appear in the H155A CDO MCD spectrum (see Figure 2). The features of the Cys-bound H155A Fe(III)CDO fraction (which appear at < 28,000 cm^{-1}) are only slightly shifted from their WT counterparts. In contrast, those displayed by the Cys-bound Fe(II)CDO fraction are sufficiently blue-shifted in the variant spectrum that only the lower-energy component of the pair of WT Fe(II)CDO features is observed. Despite these differences, the appearance of MCD features in the near-UV region upon exposure of H155A Fe(II)CDO to Cys provides direct evidence for the formation of an enzyme-substrate complex similar to that of the WT enzyme. This conclusion is further supported by the previous observation that H155A CDO is catalytically active, albeit at a reduced (~100-fold) rate relative to the WT protein.[3]

The EPR spectra obtained for as-isolated WT and H155A CDO in the presence of Cys (Figure 3) are very similar. Because only the Fe(III)CDO fraction can be observed in perpendicular-mode X-band EPR experiments, this result indicates that removal of the H155 side chain has minimal effects on the electronic structure of the Cys-bound oxidized enzyme. Both EPR spectra in Figure 3 are characteristic of high-spin Fe(III) species with nearly rhombic symmetry (for EPR fit parameters, see Table S1 of the Supporting Information). Thus, consistent with the MCD data presented above, our EPR data indicate that the geometric and electronic structures of the Cys-bound Fe(III)CDO active site are insignificantly affected by the H155A substitution. Interestingly, however, the EPR signal of the Cys-adduct of H155A Fe(III)CDO is noticeably broadened due to increased g-strain, suggesting that the conformation of the enzyme-substrate complex is less tightly controlled in the variant.

Exposure of as-isolated H155A CDO to Sec leads to the appearance of features in the MCD spectrum consistent with direct Se_{Sec}-ligation to the Fe center (see Figure 2). As in the case of Cys-bound Fe(II)CDO, the MCD features associated with the reduced fraction of Sec-bound active sites undergo a substantial blue-shift in response to the H155A substitution. A small blue-shift is also observed for the features arising from the Sec-bound Fe(III)CDO fraction, even though their Cys-derived counterparts appear to be largely unaffected by the H155A substitution (*vide supra*). However, this difference presumably stems from the fact that the MCD features of Sec-bound Fe(III)CDO are considerably more intense and better resolved than those of the Cys-bound oxidized enzyme, which allows for a more precise determination of band shifts when the substrate analogue is used. Collectively, our results indicate that exposure of H155A Fe(II)CDO and Fe(III)CDO to Cys or Sec leads to the formation of enzyme-substrate complexes that are similar to, but not identical with, those of the WT enzyme, with the larger differences involving the Fe(II)-bound fraction.

3.2 NO adducts of Cys- and Sec-Fe(II)CDO

While most electronic transitions appear at higher energies for Cys-and Sec-bound H155A Fe(II)CDO than for the corresponding WT species, minimal spectral differences are observed between the corresponding NO adducts. Specifically, the new features observed upon binding of NO to Cys-bound or Sec-bound H155A Fe(II)CDO in the 10,000–28,000 cm^{-1} range are nearly identical to those displayed by the analogous WT CDO species in terms of both their energies and relative intensities (see Figure 2, where features appearing at > 28,000 cm^{-1} are attributed to Cys- or Sec-bound active sites that did not react with NO). Thus, on the basis of our previous Abs and MCD band assignments for the nitrosyl adducts of the WT enzyme,[20] we can conclude that neither the donor (i.e., the Fe 3dxy, 3dxz, and 3dyz-based) nor the acceptor (unoccupied NO π*-based) molecular orbitals (MOs) for these transitions are significantly affected by the H155A substitution. Consistent with this conclusion, the g-values and ^{14}N hyperfine coupling constant obtained from fits of the EPR spectra of the (NO/Cys) adducts of H155A and WT Fe(II)CDO are also extremely similar, though a slightly larger g-spread is observed for the former complex (see Figure 4 for spectra and Table S2 of the Supporting Information for fit parameters). Hence, the preference of the (NO/Cys) adduct of WT Fe(II)CDO to adopt an unusual S=1/2 ground

state (with the single unpaired electron residing in an NO π*-based MO that is weakly σ-bonding with the Fe center)[19] persists upon the removal of the H155 imidazole group.

3.3 Cys- and Sec-Fe(III)CDO in the Presence of Azide

We have previously shown that even when a large molar excess of azide is added to Cys- or Sec-bound Fe(III)-WT CDO, this $O_2^{\bullet-}$ analogue binds to only a small fraction of active sites to form an S=1/2 inner-sphere complex, which precludes a direct characterization of this complex by MCD spectroscopy[17]. The very modest shifts of the MCD features that are observed upon exposure of Cys- or Sec-bound WT Fe(III)- CDO to azide can be attributed to azide occupying a pre-binding site formed in part by the guanidyl side chain of residue R60.[17] Exposing Cys- or Sec-bound H155A Fe(III)CDO to azide also results in modest MCD band shifts (Figure S2 of the Supporting Information); however, the magnitude of these shifts is greater than in the case of the WT enzyme. This finding is consistent with a less-rigidly bound Cys ligand in the absence of the H155 imidazole group, which allows perturbations to the pre-binding site to be relayed more effectively to the Fe center.

4. Computational Results

4.1 General Approach

On the basis of the spectroscopic data presented above and our previous studies of WT CDO, the following models were generated for both H155A and WT CDO via whole-protein QM/MM geometry optimizations: S=2 (Cys)-Fe(II)CDO, S=2 (H_2O/Cys)-Fe(II)CDO, S=5/2 (OH^-/Cys)-Fe(III)CDO, and S=1/2 (NO/Cys)-Fe(II)CDO, as well as the S=0, S=1, and S=2 (O_2/Cys)-FeCDO adducts. With the exception of the dioxygen adducts, the analogous Sec-bound adducts were also investigated, but because the results were often similar to those obtained for the Cys-adducts, only cases where major differences were observed are discussed below. The computational models were validated on the basis of a comparison of the optimized metric parameters with X-ray crystallographic data (where available) and the calculation of relevant spectroscopic observables; namely, the energies and Abs intensities of electronic transitions as well as EPR parameters (where applicable). Relevant bond distances for the Cys-bound species considered in this work are presented in Table 1, and analogous data for the Sec-bound species are provided in Table S3 of the Supporting Information.

4.2 Cys-Fe(II)CDO Adducts

Previous crystallographic studies revealed that Cys-bound WT Fe(II)CDO exhibits a distorted trigonal bipyramidal geometry about the Fe center with an open coordination site trans to His86 (see Figure 1).[14, 20] Because no X-ray crystallographic information about the active site coordination environment of Cys-bound H155A Fe(II)CDO is currently available, we considered both five-coordinate models and six-coordinate models additionally featuring an exogenous water ligand for the Cys- and Sec-adducts of H155A Fe(II)CDO (see Table 1 for relevant bond lengths and angles for these models). For comparison, analogous six-coordinate Cys-bound and Sec-bound models were also generated for WT Fe(II)CDO. However, in these cases the water molecule that was initially placed within bonding distance of the Fe center gradually moved away during the geometry optimization to yield five-

coordinate species with Fe-O_{water} distances of > 4 Å, consistent with the X-ray crystal structure of Cys-bound WT Fe(II)CDO (Figure 1).

A comparison of the SCF energies for the QM region of the optimized whole-protein models of substrate-bound reduced H155A CDO reveals that the six-coordinate (H_2O/Cys)-Fe(II) complex is more stable than its five-coordinate Cys-only bound analogue by ~39 kcal/mol (note that this value only provides a rough estimate of the binding energy and ignores any entropic contributions). Similarly, the (H_2O/Sec)-Fe(II) complex is favored over the five-coordinate Sec-only model by ~51 kcal/mol. The most obvious difference between the five- and six-coordinate Cys-bound H155A CDO models (other than the absence of the H_2O ligand in the former) involves the bond angles about the Fe center, with τ parameters of 0.46 and 0.19, respectively (where τ = 1 describes a trigonal bipyramidal geometry and τ = 0 signifies octahedral or square pyramidal coordination[40]). Binding of a weakly donating water ligand to the Fe center also causes the Fe–S_{Cys} bond and the Fe–N_{H88} bond trans to it to lengthen substantially (by 0.15 and 0.08 Å, respectively). The other Fe-ligand bond distances change by < |0.05| Å upon water binding, and the hydrogen bonding interactions between the Cys substrate carboxylate group and residues Y157 and R60 are largely unperturbed. The atoms of the Cys portion of the C93-Y157 cross-link also adjust in response to the binding of water to the active site, moving more significantly out of the Tyr157 plane (where the tyrosine ring plane is defined by the positions of the two Cδ atoms and Cζ) when both water and Cys are present at the Fe center. Specifically, in the six-coordinate model the S_{Cys} and $C\beta_{Cys}$ are displaced from the Tyr plane by 0.35 and 0.17 Å, respectively, versus 0.28 and 0.01 Å in the five-coordinate model.

Because Cys-bound WT Fe(II) CDO has been crystallographically shown to possess a five-coordinate Fe center,[14] the experimental Abs spectrum for this species can be compared to the INDO/S-CI predicted spectrum for the QM/MM optimized five-coordinate model active site to aid in the validation of our computational methodology. As shown in Figure S3 of the Supporting Information, the INDO/S-CI computed Abs spectrum for Cys-bound WT Fe(II)CDO exhibits a pair of intense features in the 35,000–40,000 cm^{-1} range that arise from transitions containing substantial S→Fe(II) CT character, in excellent agreement with our MCD data obtained for WT Cys-Fe(II)CDO. The computed Abs spectrum for the five-coordinate H155A Cys-Fe(II)CDO model is almost superimposable on that predicted for the corresponding WT CDO model, as expected on the basis of the highly similar active site regions of these models. In contrast, the INDO/S-CI computed Abs spectrum for the six-coordinate H155A (H_2O/Cys)-Fe(II)CDO model is noticeably blue-shifted from the other two spectra, which concurs nicely with the MCD spectral changes caused by the H155A substitution (Figure 2). For this reason, along with the fact that our QM/MM computations predict the (H_2O/Cys) adduct of H155A Fe(II)CDO to be more stable than the five-coordinate Cys-only adduct with the water molecule residing outside of the Fe coordination sphere (*vide supra*), we conclude that Cys-bound H155A Fe(II)CDO features a six-coordinate Fe center. The striking blue-shifts of the S_{Cys}→Fe(II) and Se_{Sec}→Fe(II) CT transitions of Cys- and Sec-bound H155A Fe(II)CDO, respectively, in response to the H155A substitution can, therefore, be attributed to the decreased Lewis acidity of the Fe(II) ion in the variant due to coordination of an additional ligand.

Although the five-coordinate H155A Cys-Fe(II)CDO active site model is predicted to be less stable than the corresponding six-coordinate adduct, a comparison of the five-coordinate WT and H155A Cys-Fe(II)CDO models provides clues as to how the WT enzyme retains an open coordination site for O_2 binding in the Cys-bound form. Both of these models converged to very similar geometries, with Fe–ligand bond lengths in close agreement with those observed in a recently published crystal structure (see Table 1).[14] The coordination site trans to H86 is clearly open, with the Cys sulfur, Fe center, and nitrogen of H88 forming a "bite angle" of 143.5° for both species. Three hydrogen-bonding interactions between the protein matrix and the carboxylic acid group of the substrate Cys are found in both active site models; namely, two with the guanidyl group of R60 and one with the phenol of Y157. Experimental support for the existence of such stabilizing interactions with the Cys substrate carboxylate is provided by the fact that the relative positioning of the H-bond donating residues R60 and Y157 are similar in our optimized models and the WT CDO crystal structure. One of the most notable differences between the five-coordinate WT and H155A Cys-Fe(II)CDO models involves the relative positions of the atoms in the C-Y cross-link. In the WT model, both the S_{Cys} and $C\beta_{Cys}$ atoms are essentially coplanar with the atoms of the Y157 ring. In contrast, in the five-coordinate H155A Cys-Fe(II)CDO model the sulfur atom is displaced from this plane by 0.28 Å, allowing more room for water to bind to the Fe center without steric clashes.

It is also instructive to compare the active site models for the catalytically-relevant six-coordinate H155A (H_2O/Cys)-Fe(II)CDO and five-coordinate WT Cys-Fe(II)CDO species. A particularly obvious difference between these models involves the orientation of C93-Y157 cross-link. In the WT CDO model, the phenolic oxygen is situated such as to engage in a hydrogen-bonding interaction with H155 (O¨¨H distance of 2.26 Å) and the S and Cβ atom of C93 are nearly coplanar with the phenol ring of Y157 (out-of-plane displacements of 0.03 and 0.06 Å, respectively). In the absence of the H155 side chain (and thus presence of both Cys and water at the Fe center), the atoms of the cross-link reorient, with the S and Cβ of C93 moving to ~0.35 and ~0.17 Å above the Y157 ring plane, respectively. This permits the formation of a relatively short (2.20 Å) hydrogen bond between the sulfur of C93 and a hydrogen on the water ligand that is absent in the WT Cys-Fe(II) CDO model. However, despite this distortion of the cross-link in the variant, the hydrogen-bond distance between Y157 and the substrate Cys is similar as in WT CDO, due to the ability of the phenolic hydrogen to rotate out of the ring plane. Very similar geometric trends (including hydrogen-bond distances and cross-link planarity) are predicted to exist between the WT Sec-Fe(II)CDO and H155A (H_2O/Sec)-Fe(II)CDO models.

Despite the different coordination number adopted by the iron atom in the active site models of the catalytically relevant WT Cys-Fe(II)CDO and H155A (H_2O/Cys)-Fe(II)CDO species, the DFT-computed electronic structures for these models show only modest differences. Both species are predicted to possess a high-spin Fe(II) center, as all five Fe 3d-based spin up (α) molecular orbitals (MOs) are occupied, while only one of the Fe 3d-based spin down (β) MOs is occupied (see Figure 6). Although in the H155A Cys-Fe(III)CDO model a water molecule occupies the open coordination site that is present in the in the WT model, the relative energies of the unoccupied Fe 3d-based β-MOs exhibit relatively small differences.

Note, however, that a direct comparison of these MO energies is complicated by the fact that numerous unoccupied β-MOs contain significant Fe 3d orbital character.

4.3 (OH^-/Cys)-Fe(III)CDO Adducts

On the basis of recent spectroscopic and computational studies, we have concluded that the Cys-adduct of WT Fe(III)CDO additionally features a hydroxide ligand to complete a distorted octahedral coordination environment at the Fe(III) center.[21] For this reason, an analogous adduct was generated computationally for the H155A variant via whole-protein QM/MM geometry optimization. As shown in Table 1 and Figure 5, the H155A and WT (OH^-/Cys)-Fe(III)CDO active site models exhibit only minor geometric differences. The Fe–ligand bond lengths are nearly identical in the two models, while one the two R60···Cys hydrogen-bond distances lengthen by 0.13 Å in response to the H155A substitution. This suggests the Cys substrate is granted slightly greater conformational freedom in the H155A (OH^-/Cys)-Fe(III)CDO complex, consistent with the increased g-strain observed in the EPR spectrum of this species (*vide supra*). Additionally, as in the case of the Cys-bound Fe(II)CDO species, the relative positioning of the C93-Y157 cross-link differs between the (OH^-/Cys) adducts of WT and H155A Fe(III)CDO, with the S_{Cys} and Cβ atoms being displaced from the Tyr ring plane by 0.50 and 0.50 Å, respectively in the WT model and by 0.14 and 0.23 Å, respectively in the H155A model. While in the reduced state the driving force for distorting the C-Y cross-link in the variant is the formation of a hydrogen bond to the coordinated water (*vide supra*), neither of the (OH^-/Cys)-Fe(III)CDO models features a hydrogen-bond donor to the hydroxide ligand. Instead, in the oxidized state the magnitude of the displacement of the S_{Cys} and Cβ atoms from the Tyr ring plane is largely dictated by the strength of the H-bonding interaction between the phenolic oxygen of Y157 and residue 155. As no such H-bond is present in the H155A variant, the Y157 ring can adopt a less strained conformation, yielding bond angles more consistent with sp^2 hybridization.

The computed electronic structures for the (OH^-/Cys)-Fe(III)CDO active site models are only weakly affected by the geometric differences caused by the H155A substitution (see Figure 7), as required experimentally by our MCD and EPR data (see Figures 2 and 3). However, the highest occupied molecular orbital (HOMO) and HOMO-1 are slightly stabilized in energy in the variant, while the energies of the Fe 3d-based β-MOs are essentially unperturbed. As a result, the energy differences between the donor and acceptor orbitals for the key electronic transitions are expected to increase slightly from the WT to the H155A (OH^-/Cys)-Fe(III)CDO adducts, which is consistent with our MCD data (Figure 2) and INDO/S-CI predicted Abs spectra (Figure S4 of the Supporting Information).

4.4 (NO/Cys)-Fe(II)CDO Adducts

The geometries of the computationally-derived models for the (NO/Cys)-adducts of WT and H155A Fe(II)CDO are quite similar, with the only major differences concerning the two hydrogen bonds between the Cys carboxylic acid and the R60 guanidyl group (which change by +0.07 Å and −0.16 Å from WT to H155A CDO) and the relative positioning of the S_{Cys} and $C\beta_{Cys}$ cross-link atoms (which are much less displaced from the Tyr plane in the variant). Additionally, the bond angle formed between the nitrogen of the NO ligand, Fe, and the nitrogen of the His ligand trans to the NO binding site increases slightly from 171°

to 176° in the H155A model. The orientation of the NO ligand also differs between the two models, though the lack of hydrogen bonds involving this ligand suggests that changes in the S_{Cys}–Fe–N–O dihedral angle come at a low energetic penalty.

Despite the larger differences in the active site geometries of the (NO/Cys)-Fe(II)CDO adducts as compared to the (OH^-/Cys)-Fe(III)CDO adducts of the WT and H155A enzymes, the computed electronic structures for the nitrosyl adducts are very similar (Figure 8), consistent with our MCD and EPR data (Figures 2 and 4, respectively). In particular, the composition of the formally singly-occupied molecular orbital (SOMO), which corresponds to the filled counterpart of the in-plane (i.p.) NO π*-based β-MO oriented in the Fe–N–O plane, is essentially identical for the WT and H155A (NO/Cys)-Fe(II)CDO species, as stipulated by their highly similar EPR spectra. Although the β-MOs of the H155A (Cys/NO)-Fe(II)CDO adduct are slightly destabilized in energy relative to their WT counterparts, all orbitals undergo a relatively uniform shift such that the energetic differences between the donor and acceptor orbitals for the electronic transitions responsible for the dominant MCD features remain essentially unchanged. Nonetheless, minor differences in the relative magnitudes of the Fe–NO σ- and π-bonding interactions between WT and H155A (Cys/NO)-Fe(II)CDO do exist, as revealed by the slightly larger energetic splitting between the unoccupied NO π*-based β-MOs in the variant.

5. Discussion

The role of the C93-Y157 cross-link in CDO has puzzled researchers since its identification in the first X-ray crystal structure of the enzyme.[13] From a recent EPR investigation of the (CN^-/Cys)-Fe(III)CDO adducts of as-isolated and fully-cross-linked WT enzyme it was suggested that the phenol group of Y157 engages in a hydrogen-bonding interaction with the substrate Cys carboxylic acid that is key for the proper positioning of the latter.[3] Additionally, the sulfur of C93 could provide steric bulk to the active site pocket, potentially modulating the orientation in which any exogenous sixth ligand (including O_2) binds to the Fe center.[3] The phenol of Y157 is both a hydrogen-bond donor to the substrate and a hydrogen-bond acceptor from the H155 imidazole ring, so its position within the active site pocket is carefully adjusted. On the basis of the results obtained in the present study, we suggest an additional role for H155 in tuning the relative positioning of the C-Y cross-link within the active site pocket. In the absence of the H155 imidazole side chain, the cysteine portion of the C-Y cross-link is substantially more co-planar with the Tyr ring, except in the catalytically active, Cys-bound Fe(II)CDO species where the opposite is the case.

It is intriguing that the WT Cys-Fe(II)CDO adduct is a five-coordinate species with an open coordination site for O_2 binding, whereas the H155A variant appears to retain one of the originally bound water ligands upon Cys binding to form an octahedrally coordinated Fe(II) complex. Although the removal of the H155 side chain may seem to be a fairly modest perturbation, the absence of this polar side chain allows neighboring residues to reorient within the active site pocket. The binding of an additional ligand to the five-coordinate Fe(II) center requires the equatorial His–Fe–His bond angle to contract by ~10°, forcing the Fe atom to move ~0.5 Å closer to the atoms of the C93-Y157 cross-link. In WT CDO the cross-link atoms are locked in place through H-bonding interactions with the H155 side-

chain, which effectively precludes water from binding to the Fe center. Alternatively, in the H155A CDO variant the cross-link atoms are sufficiently free to move to accommodate the structural changes required for water binding to the active site. Thus, the interplay between the H155, Y157, and C93 side chains appears to play a key role in controlling the coordination environment about the Fe(II) center.

The preference of WT Fe(II)CDO to form a five-coordinate Cys-adduct has obvious implications for the catalytic mechanism employed by this enzyme. As the Fe(II) center retains an open coordination site upon Cys-coordination, dioxygen can enter the first coordination sphere without having to displace another ligand. Additionally, the binding of O_2 to the active site prompts the movement of the Fe center away from the H155 residue side chain, relieving any steric clashes that might otherwise have been present. Alternatively, in the case of Cys-bound H155A Fe(II)CDO a ligand displacement is required to permit O_2 binding to the Fe atom, which may help explain the lower catalytic activity displayed by this enzyme variant. To evaluate this possibility, the relative O_2 binding affinities of WT and H155A Fe(II)CDO were estimated from the difference in SCF energies between the Cys-bound and (O_2/Cys)-bound Fe(II)CDO models (note that because the enzyme models for the WT and variant enzymes contain differing numbers of atoms, a comparison of their absolute energies is meaningless). We have previously evaluated the energies for three spin states of WT (O_2/Cys)-Fe(II)CDO and proposed that this species has a quintet ground state [due to ferromagnetic coupling between an intermediate spin Fe(III) ion and a superoxo-based radical], with a computed energy ~9 kcal/mol lower than the five-coordinate Cys-bound complex and free $^3O_2$.[20] The results obtained from analogous computations for the initial O_2-bound intermediate of Cys-bound H155A Fe(II)CDO are compared to those reported for the WT enzyme in Figure 9.

All three spin states for the six-coordinate H155A (O_2/Cys)-Fe(II)CDO adduct investigated in this work are significantly closer in energy to the five-coordinate than the six-coordinate Cys-bound model and free $^3O_2$ (see Figure 9). Because the six-coordinate H155A (H_2O/Cys)-Fe(II)CDO adduct is predicted to be stabilized over the five-coordinate Cys-adduct by ~39 kcal/mol, a large energetic penalty is therefore predicted for the binding of O_2 to the (H_2O/Cys)-bound active site of H155A Fe(II)CDO (~34 kcal/mol for the $^5\mathbf{A'}$ to $^5\mathbf{B'}$ pathway). Although our approach ignores entropic contributions to the free energy of O_2 binding, which would lower the energy of the (O_2/Cys) adduct for H155A CDO relative to that of the WT complex due to the release of the water molecule originally bound to the Fe(II) ion in the variant, these contributions are unlikely to compensate for the large energetic penalty associated with the $^5\mathbf{A'}$ to $^5\mathbf{B'}$ conversion. Hence, we propose that the drastically reduced enzymatic activity of the H155A variant (< 2% of WT)[3] is due, at least in part, to a largely reduced O_2 binding affinity of the corresponding Cys-Fe(II)CDO adduct.

Although the (O_2/Cys) adducts for both WT and H155A Fe(II)CDO are predicted to possess a quintet ground state ($^5\mathbf{B}$ and $^5\mathbf{B'}$, respectively), the electron configuration differs between the two models. The WT species has previously been shown to be best described as an intermediate spin Fe(III) ion coupled ferromagnetically to a superoxide-based radical.[20] Alternatively, the computed electronic structure for the (O_2/Cys) adduct of H155A Fe(II)CDO is more consistent with a high spin Fe(II) ion bound to a singlet dioxygen

moiety. This distinct electron distribution probably reflects the unusual binding mode adopted by the dioxygen moiety in this species, which was found to be end-on to the Fe–S bond even if the O_2 moiety was initially placed within bonding distance of the Fe(II) atom prior to the QM/MM geometry optimization. A similar configuration of substrate O_2 was previously seen in a crystal structure of WT CDO in the presence of Cys and air (PDB code 3ELN)[42], though it was later found that this species does not represent a true reaction intermediate.[43] It is important to note that even though the unusual O_2 binding mode may contribute to the high relative energy of the $^5\mathbf{B'}$ intermediate, the relative energies of the $^1\mathbf{B'}$ and $^3\mathbf{B'}$ species are also ~25 kcal/mol higher than those of their structurally nearly identical WT counterparts ($^1\mathbf{B}$ and $^3\mathbf{B}$, respectively).

6. Conclusions

Although the presence of the H155 side chain appears to have modest to no effects on the geometric and electronic structures of the CDO active site in some states, a drastic difference is seen for the catalytically relevant Cys-bound Fe(II) center. In the presence of the H155 side chain (i.e., in WT CDO), X-ray crystallographic and computational results indicate that the Cys-bound WT Fe(II)CDO active site adopts a distorted trigonal bipyramidal coordination geometry, which allows the reaction with O_2 to proceed with a low activation energy barrier, and thus a relatively fast rate (the overall rate constant for Cys oxidation by CDO is 8.6 s^{-1}). Remarkably, the introduction of a third-sphere amino acid substitution to generate the H155A CDO variant causes a decrease in the turnover rate by almost 2 orders of magnitude. While the molecular basis for this drastic reduction in the overall rate constant for Cys oxidation was previously unknown, the spectroscopic and computational data obtained in the present study lead us to propose that a six-coordinate (H_2O/Cys)-Fe(II)CDO complex is formed in the variant due to the ability of the crosslink to accept a hydrogen bond from the coordinated H_2O molecule in the absence of the H155 side chain. Thus, for O_2 binding to this complex to occur, the coordinated water molecule must first be removed to form a transient five-coordinate Fe(II) species (likely in an entropically-controlled process that depresses the rate at which O_2-binding proceeds). The H155 side chain thus appears to assume a key role in the CDO catalytic cycle by discouraging the binding of a water molecule in the position where O_2 must bind to the Cys-bound Fe(II)CDO complex to initiate catalysis. Because in the non-cross-linked WT enzyme the S atom of the C93 side chain is granted even more conformational freedom than in the H155A CDO variant, it is tempting to speculate that the binding of a water molecule to the Cys-bound Fe(II)CDO complex is also responsible for the low catalytic activity of CDO lacking the cross-link. In this scenario, replacement the C93 with a residue that is unable to serve as a hydrogen-bond acceptor and thus to stabilize coordinated solvent should restore full activity, consistent with the results that have recently been reported for C93G CDO.[44]

Supplementary Material

Refer to Web version on PubMed Central for supplementary material.

Acknowledgments

Funding Source: This work was supported by the National Institutes of Health grant GM 64631 (T.C.B.), the National Science Foundation grant MCB-0843239 (B.G.F.), and the National Science Foundation grant CHE-0840494 (computational resources)

Abbreviations

CDO	cysteine dioxygenase
Cys	cysteine
Sec	selenocysteine
EPR	electron paramagnetic resonance
MCD	magnetic circular dichroism
Abs	electronic absorption
DFT	density functional theory
RT	room temperature
LT	low temperature
QM/MM	quantum mechanics/molecular mechanics
MO	molecular orbital
EDDM	electron density difference map
SCF	self-consistent field
INDO/S-CI	intermediate neglect of differential overlap/singles-configuration interaction
HOMO	highest occupied molecular orbital
LUMO	lowest unoccupied molecular orbital

References

1. Yamaguchi K, Hosokawa Y. CYSTEINE DIOXYGENASE. Methods in Enzymology. 1987; 143:395–403. [PubMed: 2821347]
2. Lombardi, Jb; Singer, TP.; Boyer, PD. CYSTEINE OXYGENASE .2. STUDIES ON MECHANISM OF REACTION WITH 18OXYGEN. Journal of Biological Chemistry. 1969; 244:1172. [PubMed: 5767301]
3. Li W, Blaesi EJ, Pecore MD, Crowell JK, Pierce BS. Second-Sphere Interactions between the C93–Y157 Cross-Link and the Substrate-Bound Fe Site Influence the O_2 Coupling Efficiency in Mouse Cysteine Dioxygenase. Biochemistry. 2013; 52:9104–9119. [PubMed: 24279989]
4. Stipanuk MH, Ueki I. Dealing with methionine/homocysteine sulfur: cysteine metabolism to taurine and inorganic sulfur. Journal of Inherited Metabolic Disease. 2011; 34:17–32. [PubMed: 20162368]
5. Ueki I, Roman HB, Valli A, Fieselmann K, Lam J, Peters R, Hirschberger LL, Stipanuk MH. Knockout of the Murine Cysteine Dioxygenase Gene Results in Severe Impairment in Ability to Synthesize Taurine and an Increased Catabolism of Cysteine to Hydrogen Sulfide. American Journal of Physiology-Endocrinology and Metabolism. 2011; 301:E668–E684. [PubMed: 21693692]

6. Slivka A, Cohen G. BRAIN ISCHEMIA MARKEDLY ELEVATES LEVELS OF THE NEUROTOXIC AMINO-ACID, CYSTEINE. Brain Research. 1993; 608:33–37. [PubMed: 8495346]

7. Pean AR, Parsons RB, Waring RH, Williams AC, Ramsden DB. TOXICITY OF SULFUR-CONTAINING-COMPOUNDS TO NEURONAL CELL-LINES. Journal of the Neurological Sciences. 1995; 129:107–108. [PubMed: 7595598]

8. Heafield MT, Fearn S, Steventon GB, Waring RH, Williams AC, Sturman SG. Plasma Cysteine and Sulphate Levels in Patients with Motor Neurone, Parkinson's and Alzheimer's Disease. Neuroscience Letters. 1990; 110:216–220. [PubMed: 2325885]

9. Gordon C, Bradley H, Waring RH, Emery P. ABNORMAL SULFUR OXIDATION IN SYSTEMIC LUPUS-ERYTHEMATOSUS. Lancet. 1992; 339:25–26. [PubMed: 1345954]

10. Emery P, Bradley H, Gough A, Arthur V, Jubb R, Waring R. Increased prevalence of poor sulphoxidation in patients with rheumatoid arthritis: effect of changes in the acute phase response and second line drug treatment. Annals of the Rheumatic Diseases. 1992; 51:318–320. [PubMed: 1575574]

11. Brait M, Ling SZ, Nagpal JK, Chang XF, Park HL, Lee J, Okamura J, Yamashita K, Sidransky D, Kim MS. Cysteine Dioxygenase 1 Is a Tumor Suppressor Gene Silenced by Promoter Methylation in Multiple Human Cancers. Plos One. 2012; 7

12. Jeschke J, O'Hagan HM, Zhang W, Vatapalli R, Calmon MF, Danilova L, Nelkenbrecher C, Van Neste L, Bijsmans I, Van Engeland M, Gabrielson E, Schuebel KE, Winterpacht A, Baylin SB, Herman JG, Ahuja N. Frequent Inactivation of Cysteine Dioxygenase Type 1 Contributes to Survival of Breast Cancer Cells and Resistance to Anthracyclines. Clinical Cancer Research. 2013; 19:3201–3211. [PubMed: 23630167]

13. McCoy JG, Bailey LJ, Bitto E, Bingman CA, Aceti DJ, Fox BG, Phillips GN. Structure and Mechanism of Mouse Cysteine Dioxygenase. Proceedings of the National Academy of Sciences of the United States of America. 2006; 103:3084–3089. [PubMed: 16492780]

14. Driggers CM, Cooley RB, Sankaran B, Hirschberger LL, Stipanuk MH, Karplus PA. Cysteine Dioxygenase Structures from pH 4 to 9: Consistent Cys-Persulfenate Formation at Intermediate pH and a Cys-Bound Enzyme at Higher pH. Journal of Molecular Biology. 2013; 425:3121–3136. [PubMed: 23747973]

15. Gardner JD, Pierce BS, Fox BG, Brunold TC. Spectroscopic and Computational Characterization of Substrate-Bound Mouse Cysteine Dioxygenase: Nature of the Ferrous and Ferric Cysteine Adducts and Mechanistic Implications. Biochemistry. 2010; 49:6033–6041. [PubMed: 20397631]

16. Ye S, Wu Xa, Wei L, Tang D, Sun P, Bartlam M, Rao Z. An Insight into the Mechanism of Human Cysteine Dioxygenase: Key Roles of the Thioether-Bonded Tyrosine-Cysteine Cofactor. The Journal of Biological Chemistry. 2007; 282:3391–3402. [PubMed: 17135237]

17. Blaesi EJ, Fox BG, Brunold TC. Spectroscopic and Computational Investigation of Iron(III) Cysteine Dioxygenase: Implications for the Nature of the Putative Superoxo-Fe(III) Intermediate. Biochemistry. 2014; 53:5759–5770. [PubMed: 25093959]

18. Crawford JA, Li W, Pierce BS. Single Turnover of Substrate-Bound Ferric Cysteine Dioxygenase with Superoxide Anion: Enzymatic Reactivation, Product Formation, and a Transient Intermediate. Biochemistry. 2011; 50:10241–10253. [PubMed: 21992268]

19. Pierce BS, Gardner JD, Bailey LJ, Brunold TC, Fox BG. Characterization of the nitrosyl adduct of substrate-bound mouse cysteine dioxygenase by electron paramagnetic resonance: Electronic structure of the active site and mechanistic implications. Biochemistry. 2007; 46:8569–8578. [PubMed: 17602574]

20. Blaesi EJ, Gardner JD, Fox BG, Brunold TC. Spectroscopic and Computational Characterization of the NO Adduct of Substrate-Bound Fe(II) Cysteine Dioxygenase: Insights into the Mechanism of O_2 Activation. Biochemistry. 2013; 52:6040–6051. [PubMed: 23906193]

21. Blaesi EJ, Fox BG, Brunold TC. Spectroscopic and Computational Investigation of Fe(III) Cysteine Dioxygenase: Implications for the Nature of the Putative Superoxo-Fe(III) Intermediate. Biochemistry Just. 2014 Accepted Manuscript.

22. Dominy JE, Hwang J, Guo S, Hirschberger LL, Zhang S, Stipanuk MH. Synthesis of Amino Acid Cofactor in Cysteine Dioxygenase is Regulated by Substrate and Represents a Novel Post-

Translational Regulation of Activity. Journal of Biological Chemistry. 2008; 283:12188–12201. [PubMed: 18308719]

23. Dominy JE, Simmons CR, Karplus PA, Gehring AM, Stipanuk MH. Identification and characterization of bacterial cysteine dioxygenases: a new route of cysteine degradation for eubacteria. Journal of Bacteriology. 2006; 188:5561–5569. [PubMed: 16855246]
24. Crowell JK, Li W, Pierce BS. Oxidative uncoupling in cysteine dioxygenase is gated by a proton-sensitive intermediate. Biochemistry. 2014; 53:7541–7548. [PubMed: 25387045]
25. Kleffmann T, Jongkees SAK, Fairweather G, Wilbanks SM, Jameson GNL. Mass-spectrometric characterization of two posttranslational modifications of cysteine dioxygenase. Journal of Biological Inorganic Chemistry. 2009; 14:913–921. [PubMed: 19373496]
26. Siakkou E, Rutledge MT, Wilbanks SM, Jameson GNL. Correlating crosslink formation with enzymatic activity in cysteine dioxygenase. Biochimica Et Biophysica Acta-Proteins and Proteomics. 2011; 1814:2003–2009.
27. Fischer DS, Price DS. A Simple Serum Iron Method Using the New Sensitive Chromogen Tripyridyl-s-triazine. Clinical Chemistry. 1964; 10:21–31. [PubMed: 14110802]
28. Stoll S, Schweiger A. EasySpin, a comprehensive software package for spectral simulation and analysis in EPR. Journal of Magnetic Resonance. 2006; 178:42–55. [PubMed: 16188474]
29. Frisch, MJ.; Trucks, GW.; Schlegel, HB.; Scuseria, GE.; Robb, MA.; Cheeseman, JR.; Scalmani, G.; Barone, V.; Mennucci, B.; Petersson, GA.; Nakatsuji, H.; Caricato, M.; Li, X.; Hratchian, HP.; Izmaylov, AF.; Bloino, J.; Zheng, G.; Sonnenberg, JL.; Hada, M.; Ehara, M.; Toyota, K.; Fukuda, R.; Hasegawa, J.; Ishida, M.; Nakajima, T.; Honda, Y.; Kitao, O.; Nakai, H.; Vreven, T.; Montgomery, J.; JA; Peralta, JE.; Ogliaro, F.; Bearpark, M.; Heyd, JJ.; Brothers, E.; Kudin, KN.; Staroverov, VN.; Keith, T.; Kobayashi, R.; Normand, J.; Raghavachari, K.; Rendell, A.; Burant, JC.; Iyengar, SS.; Tomasi, J.; Cossi, M.; Rega, N.; Millam, JM.; Klene, M.; Knox, JE.; Cross, JB.; Bakken, V.; Adamo, C.; Jaramillo, J.; Gomperts, R.; Stratmann, RE.; Yazyev, O.; Austin, AJ.; Cammi, R.; Pomelli, C.; Ochterski, JW.; Martin, RL.; Morokuma, K.; Zakrzewski, VG.; Voth, GA.; Salvador, P.; Dannenberg, JJ.; Dapprich, S.; Daniels, AD.; Farkas, O.; Foresman, JB.; Ortiz, JV.; Cioslowski, J.; Fox, DJ. Gaussian 09, Revision C.01. Gaussian, Inc; Wallingford, CT: 2010.
30. Cornell WD, Cieplak P, Bayly CI, Gould IR, Merz KM, Ferguson DM, Spellmeyer DC, Fox T, Caldwell JW, Kollman PA. A 2ND GENERATION FORCE-FIELD FOR THE SIMULATION OF PROTEINS, NUCLEIC-ACIDS, AND ORGANIC-MOLECULES. Journal of the American Chemical Society. 1995; 117:5179–5197.
31. Lee CT, Yang WT, Parr RG. DEVELOPMENT OF THE COLLE-SALVETTI CORRELATION-ENERGY FORMULA INTO A FUNCTIONAL OF THE ELECTRON-DENSITY. Physical Review B. 1988; 37:785–789.
32. Becke AD. DENSITY-FUNCTIONAL THERMOCHEMISTRY .3. THE ROLE OF EXACT EXCHANGE. Journal of Chemical Physics. 1993; 98:5648–5652.
33. Hehre WJ, Ditchfie R, Pople JA. SELF-CONSISTENT MOLECULAR-ORBITAL METHODS . 12. FURTHER EXTENSIONS OF GAUSSIAN-TYPE BASIS SETS FOR USE IN MOLECULAR-ORBITAL STUDIES OF ORGANIC-MOLECULES. Journal of Chemical Physics. 1972; 56:2257.
34. Schafer A, Horn H, Ahlrichs R. FULLY OPTIMIZED CONTRACTED GAUSSIAN-BASIS SETS FOR ATOMS LI TO KR. Journal of Chemical Physics. 1992; 97:2571–2577.
35. Neese, F. Orca 2.9.1, An Ab Initio, DFT and Semiempirical Electronic Structure Package. 2012.
36. Schrodinger. The PyMOL Molecular Graphics System, 1.5.0.4 ed.
37. Neese F. Prediction and interpretation of the Fe-57 isomer shift in Mossbauer spectra by density functional theory. Inorganica Chimica Acta. 2002; 337:181–192.
38. Wachters AJ. GAUSSIAN BASIS SET FOR MOLECULAR WAVEFUNCTIONS CONTAINING THIRD-ROW ATOMS. Journal of Chemical Physics. 1970; 52:1033.
39. Kutzelnigg, W.; Fleischer, U.; Schindler, M., editors. The IGLO method: Ab initio calculation and interpretation of NMR chemical shifts and magnetic susceptibilities. Vol. 23. Springer-Verlag; Heidelberg. Germany: 1990.
40. Addison AW, Rao TN, Reedijk J, Vanrijn J, Verschoor GC. SYNTHESIS, STRUCTURE, AND SPECTROSCOPIC PROPERTIES OF COPPER(II) COMPOUNDS CONTAINING NITROGEN

SULFUR DONOR LIGANDS - THE CRYSTAL AND MOLECULAR-STRUCTURE OF AQUA 1,7-BIS(N-METHYLBENZIMIDAZOL-2′-YL)-2,6-DITHIAHEPTANE COPPER(II) PERCHLORATE. Journal of the Chemical Society-Dalton Transactions. 1984:1349–1356.

41. Lundblad, RL.; Macdonald, F. Handbook of Biochemistry and Molecular Biology, Fourth Edition. 4. CRC Press; 2010.
42. Simmons CR, Krishnamoorthy K, Granett SL, Schuller DJ, Dominy JE, Begley TP, Stipanuk MH, Karplus PA. A Putative Fe2+-Bound Persulfenate Intermediate in Cysteine Dioxygenase. Biochemistry. 2008; 47:11390–11392. [PubMed: 18847220]
43. Souness RJ, Kleffmann T, Tchesnokov EP, Wilbanks SM, Jameson GB, Jameson GNL. Mechanistic Implications of Persulfenate and Persulfide Binding in the Active Site of Cysteine Dioxygenase. Biochemistry. 2013; 52:7606–7617. [PubMed: 24084026]
44. Davies CG, Fellner M, Tchesnokov EP, Wilbanks SM, Jameson GNL. The Cys-Tyr Cross-Link of Cysteine Dioxygenase Changes the Optimal pH of the Reaction without a Structural Change. Biochemistry. 2014; 53:7961–7968. [PubMed: 25390690]

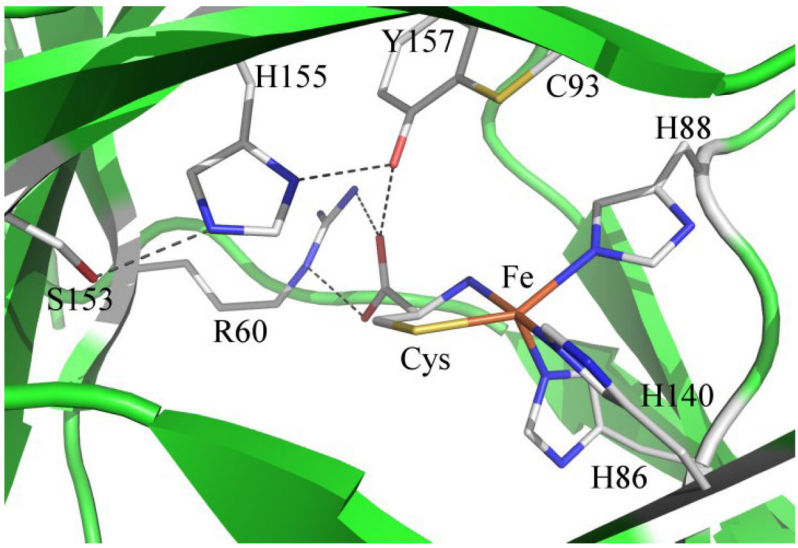

Figure 1.

Crystal structure of Cys-bound Fe(II)CDO from rat (PDB code: 4JTO, 2.00 Å resolution).[14] Potential hydrogen bonds are shown as dashed lines.

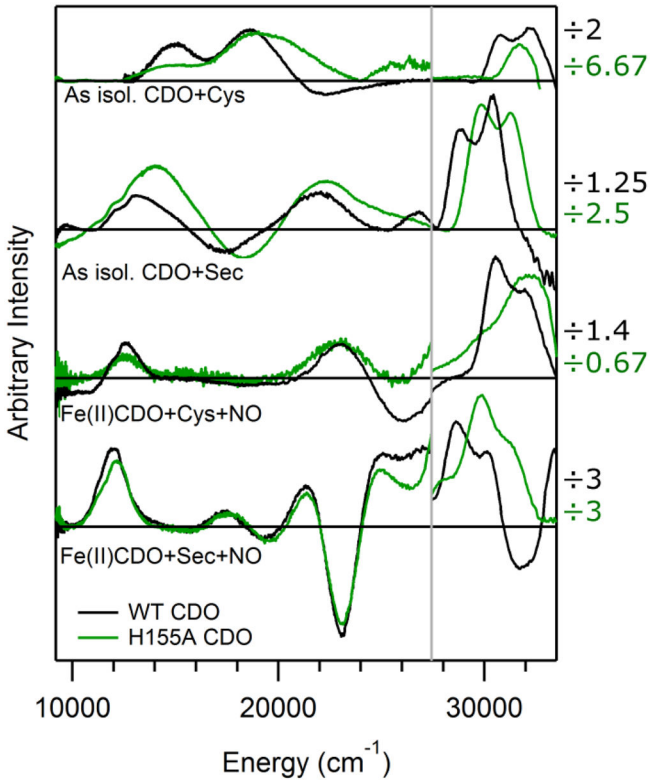

Figure 2.

MCD spectra (at 4.5 K and 7 T) of various WT (black) and H155A (green) CDO species examined in this work. Note the scale change at ~28,000 cm^{-1}, where the factors by which the intensities in the higher energy region were scaled are provided on the right.

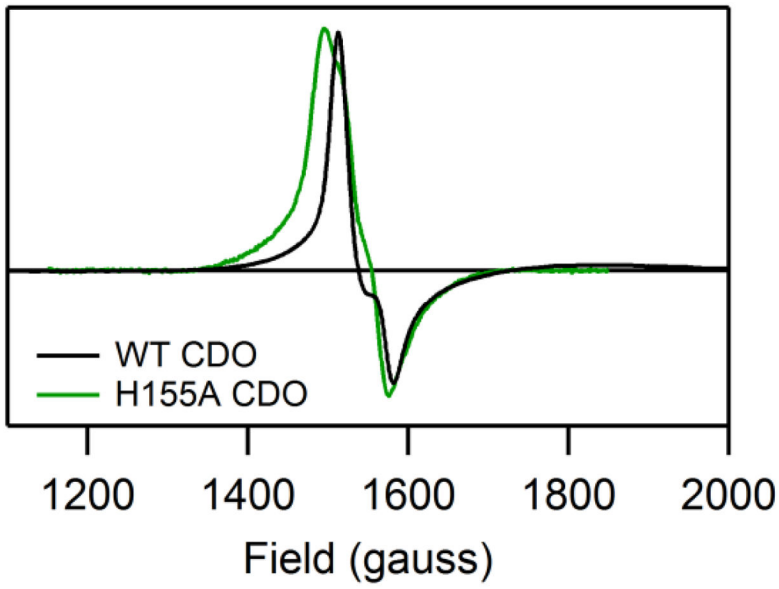

Figure 3.

X-band EPR spectra (at 20 K) of as-isolated WT and H155A CDO in the presence of Cys. No features attributable to CDO species were observed outside the region shown. For simulation parameters, see Table S1.

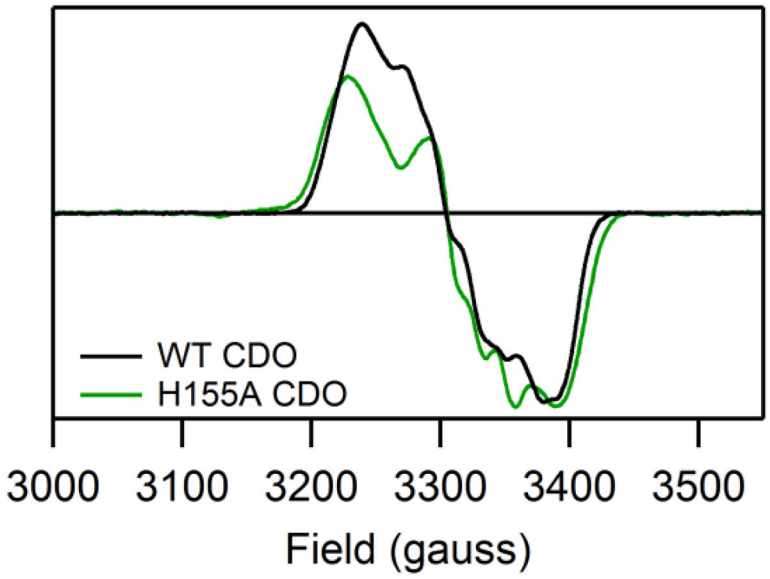

Figure 4.

X-band EPR spectra (at 20 K) of the (NO/Cys) adducts of H155A and WT Fe(II)CDO. No features attributable to CDO species were observed outside the region shown. For simulation parameters, see Table S2.

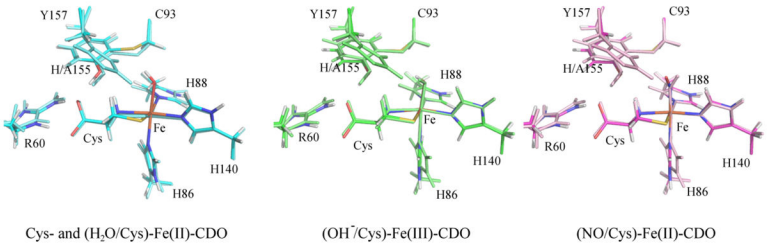

Figure 5.

Overlays of active site regions as obtained from whole-protein QM/MM optimizations, where the models in atom-specific coloring are for H155A CDO, and those with monochromatic coloring are for WT CDO. In the case of Cys-bound Fe(II) CDO, the six coordinate H155A (H_2O/Cys)-Fe(II)CDO model is shown. Backbone atoms (with the exception of the α-carbons) are hidden for clarity.

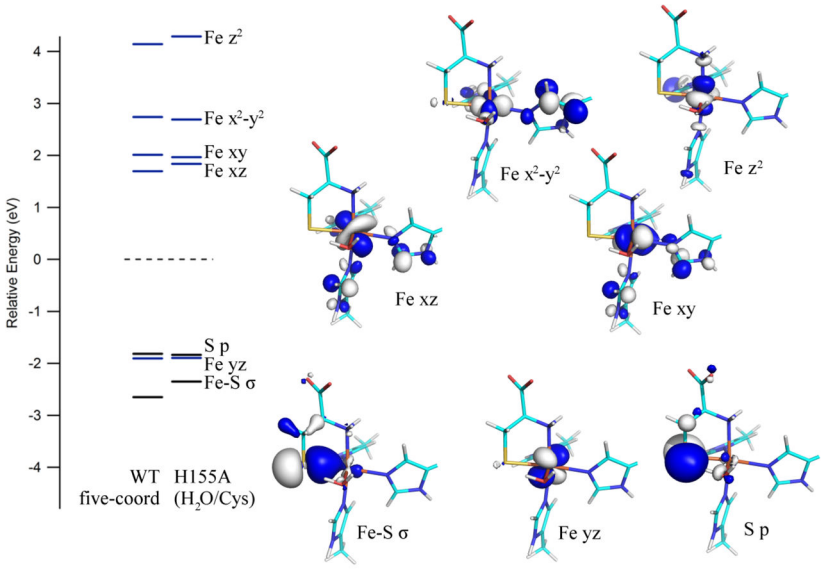

Figure 6.

DFT-computed energies of relevant spin-down MOs for the active site models of WT Cys-Fe(II)CDO and H155A (H_2O/Cys)-Fe(II)CDO. Boundary surface plots for the H155A-derived MOs are also shown. The orbital energies for both models were adjusted such that the β-HOMO (a ligand-based orbital with essentially identical compositions for both species) lies at 0 eV. Note that the primarily water-based MOs for the H155A model are present at significantly lower energies and have been omitted from this diagram.

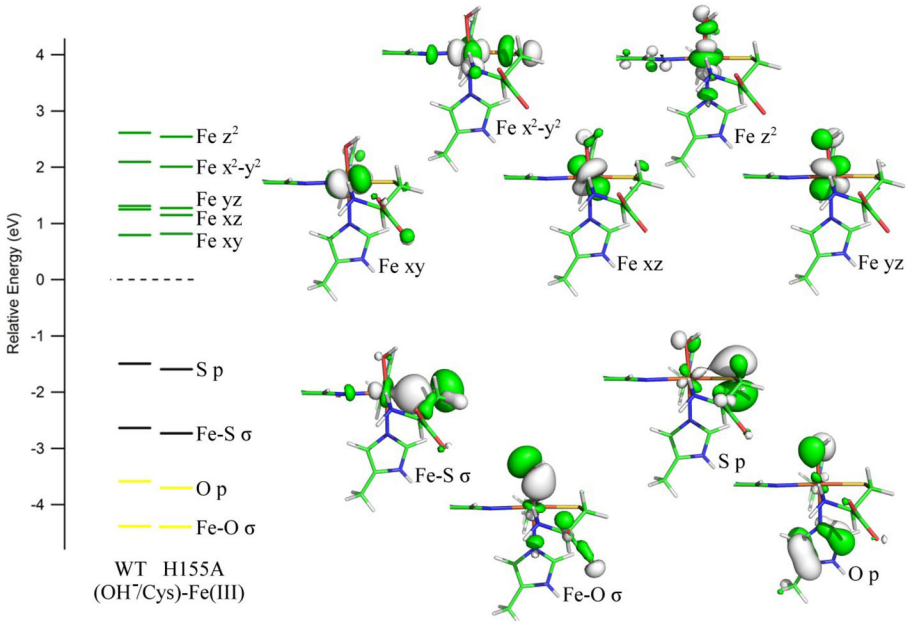

Figure 7.

DFT-computed energies of relevant spin-down MOs for the active site models of WT and H155A (OH^-/Cys)-Fe(III)CDO. Boundary surface plots for the H155A-derived MOs are also shown. The orbital energies for both models were adjusted such that the β-HOMO (a ligand-based orbital with essentially identical compositions for both species) lies at 0 eV.

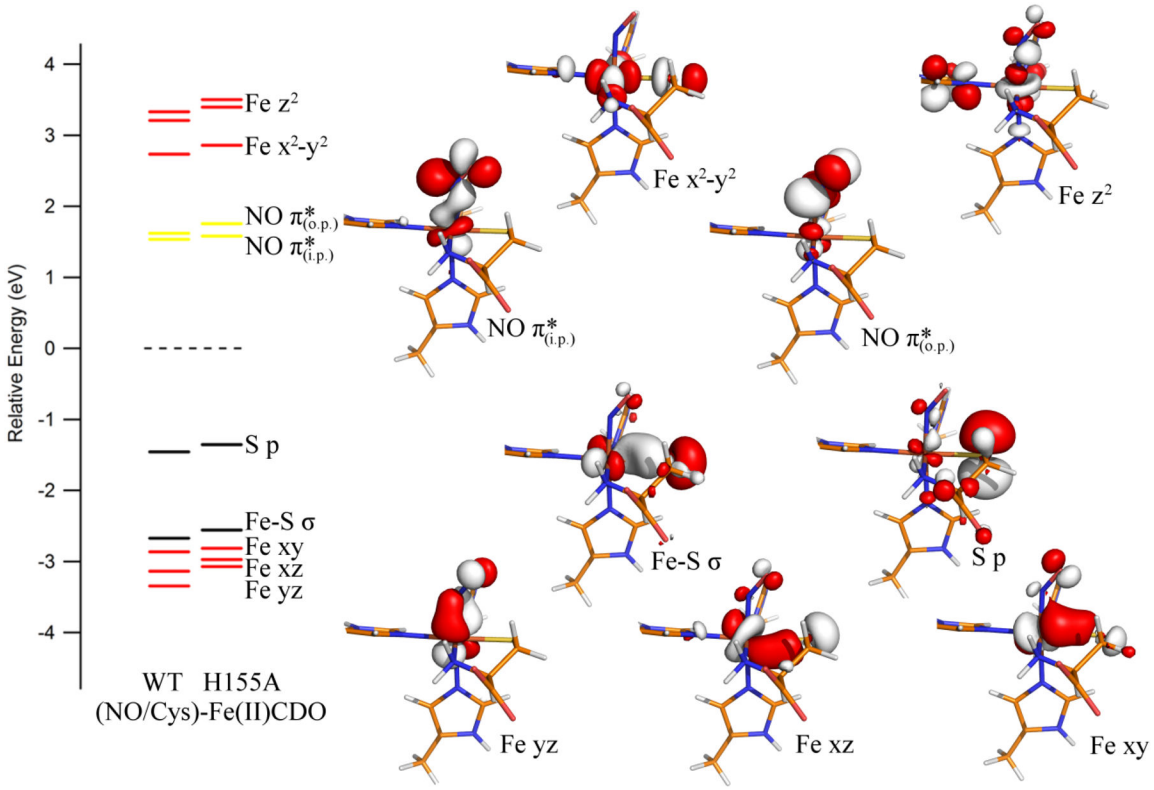

Figure 8.

DFT-computed energies of relevant spin-down MOs for the active site models of WT and H155A (NO/Cys)-Fe(II)CDO. Boundary surface plots for the H155A-derived MOs are also shown. The orbital energies for both models were adjusted such that the β-HOMO (a ligand-based orbital with essentially identical compositions for both species) lies at 0 eV.

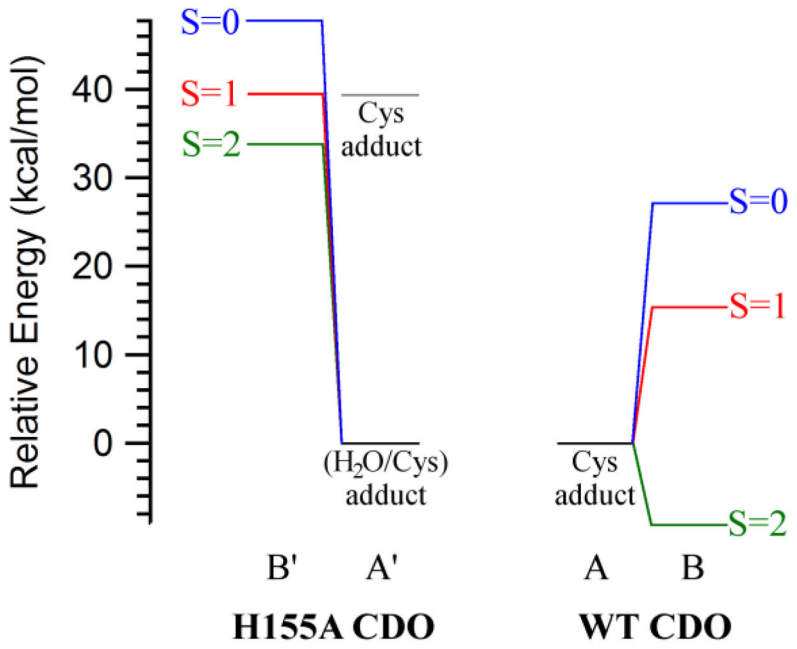

Figure 9.

Reaction coordinate diagrams showing the computed relative energies of the Cys- and (O_2/Cys)-bound species (A/A′ and B/B′, respectively) of WT and H155A Fe(II)CDO. To facilitate a direct comparison between different species, the energy of the most stable Cys-bound Fe(II)CDO adduct and free $^3O_2$ was set to zero kcal/mol in each case. For H155A CDO, the relative energies of both the five-coordinate Cys and the six-coordinate (Cys/H_2O) adducts are shown (in gray and black, respectively). Values for the WT CDO species were taken from ref 20.

Table 1

Bond distances (in Angstroms) for various Cys-bound CDO species as obtained by X-ray crystallography (4JTO) or whole-protein QM/MM optimizations (all other models listed), where X refers to the ligating atom of the sixth ligand present at the Fe center (where applicable). For the analogous Sec-bound analogues, see Table S3 of the Supporting Information

Species	Fe-N_{H86}	Fe-N_{H88}	Fe-N_{H140}	Fe-S_{Cys}	Fe-N_{Cys}	Fe-X	Cys-R60, 1	Cys-R60, 2	Cys-Y157
4JTO, WT (Cys)-Fe(II)CDO[a]	1.893	2.199	2.110	2.291	2.262	N/A	N/A	N/A	N/A
WT (Cys)-Fe(II)CDO	2.153	2.184	2.177	2.368	2.250	N/A	1.800	2.014	1.537
H155A (Cys)-Fe(II)CDO	2.158	2.198	2.172	2.372	2.256	N/A	1.717	2.134	1.552
H155A (H_2O/Cys)-Fe(II)CDO	2.205	2.273	2.142	2.521	2.278	2.311	1.734	2.188	1.552
WT (OH^-/Cys)-Fe(III)CDO	2.326	2.299	2.111	2.445	2.223	1.880	1.984	1.791	1.532
H155A (OH^-/Cys)-Fe(III)CDO	2.328	2.287	2.116	2.428	2.237	1.872	2.110	1.717	1.549
WT (NO/Cys)-Fe(II)CDO	2.113	2.110	2.013	2.369	2.115	1.769	1.772	2.008	1.529
H155A (NO/Cys)-Fe(II)CDO	2.145	2.160	2.026	2.339	2.083	1.776	1.707	2.163	1.535

[a] Crystal structure at 2.00 Å resolution, from Ref 14.